Methodology for the Evaluation of Double-Layered Microcapsule Formability Zone in Compound Nozzle Jetting Based on Growth Rate Ratio

Wei Wang

C. Leigh Herran

Nicole Coutris

Yong Huang[1]
e-mail: yongh@clemson.edu

Department of Mechanical Engineering,
Clemson University,
Clemson, SC 29634

Vladimir Mironov

Roger Markwald

Department of Regenerative Medicine
and Cell Biology,
Medical University of South Carolina,
Charleston, SC 29425

Double-layered microcapsules, which usually consist of a core (polymeric) matrix surrounded by a (polymeric) shell, have been used in many industrial and scientific applications, such as microencapsulation of drugs and living cells. Concentric compound nozzle-based jetting has been favored due to its efficiency and precise control of the core-shell compound structure. Thus far, little is known about the underlying formation mechanism of double-layered microcapsules in compound nozzle jetting. This study aims to understand the formability of double-layered microcapsules in compound nozzle jetting by combining a theoretical analysis and numerical simulations. A linear temporal instability analysis is used to define the perturbation growth rates of stretching and squeezing modes and a growth ratio as a function of the wave number, and a computational fluid dynamics (CFD) method is implemented to model the microcapsule formation process in order to determine the good microcapsule forming range based on the growth ratio curve. Using a pseudobisection method, the lower and upper bounds of the good formability range have been determined for a given materials-nozzle system. The proposed formability prediction methodology has been implemented to model a water-poly (lactide-co-glycolide) (PLGA)-air compound jetting system. [DOI: 10.1115/1.4023646]

1 Introduction

Encapsulation of micro/nano-sized droplets inside a microcapsule has been of great interest for many industrial and scientific applications. Double-layered microcapsules (or compound droplets), which usually consist of a core (polymeric) matrix surrounded by a (polymeric) shell, have been used in many applications, such as controlled release of food additives [1] and drugs [2]. Encapsulation can help isolate an unstable component from a corrosive environment, avoid decomposition of an unstable polymer due to exposure to a certain atmosphere, and deliver a given material to a particular receptor, to name a few [3]. It should be pointed out that sometimes there could be more than one core encapsulated inside a shell.

Double emulsification, followed by solvent extraction/evaporation-based hardening or ion exchange-based gelation to get a stable or solid shell structure, is the main mechanism in fabricating microcapsules. Emulsification is a process to disperse one liquid (the dispersed phase) into the other (the continuous phase) to make emulsions, such as the oil/water emulsion. Emulsification can be implemented to fabricate microcapsules using different technologies including compound or multiple concentric nozzle-based dripping/jetting [4–7], microdrop collision [8], and stirring/mixing-based bulk emulsification [9]. In compound or multiple concentric nozzle-based jetting, the coaxial nozzle set was utilized to produce a liquid core jet surrounded by an annular jet, which might be further surrounded by a nonsolvent carrier stream [7,10]. A coaxial microcapillary fluidic device was further developed to have precise control of the number of droplets encapsulated in each larger drop, allowing more than one core inside a shell structure [5]. With the assistance of an electric field, electrohydrodynamic (EHD) force facilitated microcapsule fabrication in a concentric nozzle set [4]. Microdrop collision using two inkjet nozzles was also used to make microcapsules by the collision of microdrops of an aqueous and a polymer solution, and the solvent exchange occurred as the drops contacted with each other, and finally the compound drops with polymer solution surrounded were formed [8]. Stirring/mixing-based bulk emulsification usually involved two emulsification steps: the core material was first stirred into a shell polymer solution, and then the formed emulsions were further stirred into an emulsifier-based solution, forming double emulsions [9].

Among the aforementioned technologies, compound or multiple concentric nozzle-based jetting has been favored due to its efficiency and precise control of the core-shell compound structure [7,10]. During double-layered microcapsule fabrication, it is desirable to have monodisperse microcapsules with a core material enclosed by a surrounding shell material through compound nozzle jetting. Compared with the single nozzle jetting process [11], compound jetting is more physically delicate, and the formation of double-layered microcapsule only occurs in a narrow window of fluid flow conditions and rheological parameters. Thus far, little is known about the underlying formation mechanism of double-layered microcapsules in compound nozzle jetting. As the double-layered microcapsule fabrication and size control mostly depend on the formation mechanism of microcapsules, it is thus necessary to understand the underlying mechanism of microcapsule formation in order to achieve robust microcapsule fabrication.

This study aims to propose a methodology to determine the formability of double-layered microcapsules/compound droplets during compound nozzle jetting by combining a theoretical analysis with numerical simulations. A linear temporal instability analysis has been used to define the perturbation growth rates (stretching and squeezing) and their ratio as a function of the wave number, and a computational fluid dynamics (CFD) method has been implemented to model the microcapsule formation process in order to determine the good microcapsule forming range

[1]Corresponding author.

Manuscript received May 31, 2012; final manuscript received January 4, 2013; published online April 8, 2013. Assoc. Editor: Ye Zhou.

 Copyright © 2013 by ASME

based on the growth ratio curve. The proposed approach can help to identify optimum operating conditions to produce microcapsules instead of using a trial-and-error method to obtain operating conditions for microcapsule formation. While the one core-one shell double-layered structure is studied here, it should be pointed out that the resulting knowledge also applies to multicore-one shell double layered structures.

2 Background

Droplet formation in compound nozzle dripping/jetting usually resorts to one of the two mechanisms, dripping and jetting. Generally, under the dripping mode, the direct formation of drops without a jet can be observed when a liquid is injected into another liquid below a critical value, the jetting velocity [12]. In the dripping mode, the viscous and/or gravitational force usually overcomes the surface tension force to produce the droplets close to the exit of the orifice [13], and the diameter of droplets formed [5,14] and the number of droplets encapsulated [14] in the dripping mode are dependent on the core and shell flow rates. In the jetting mode, the jet of fluid tends to break into droplets due to capillary instability, usually under some external excitation, such as acoustic excitation [7]. Generally, compound jetting is favored for its high productivity.

The compound jet breakup mechanism is more complex than that of the single jet. In compound jetting, the two fluid phases need to be synchronized to break up to form a double-layered microcapsule/compound droplet. The jet breakup synchronization has a high requirement for the viscosities and surface tensions of the jetting fluids and the flow rates. Some experimental studies have been performed to obtain the microcapsule size as a function of the flow rates of core and shell fluids [15–17]; however, there is no reported experimental effort to understand the formability of double-layered microcapsules. In addition, theoretical efforts have been implemented to understand the double-layered microcapsule formation mechanism. Tomotika [18] analytically considered the effect of the surrounding liquid in the case of a viscous jet surrounded by a viscous fluid and obtained the growth rate in the limiting case of two very viscous liquids. When the surrounding fluid has a finite thickness, a double-layered microcapsule may be formed. Sanz and Meseguer [19] analyzed the temporal instability of a compound jet using a one-dimensional inviscid model and predicted the perturbation growth rate. Shkadov and Sisoev [20] studied the instability of an axisymmetrical compound jet and found that the stability and the growth rate of disturbance were dependent on density ratio, viscosity ratio, interfacial tension ratio, Reynolds number, Weber number, and radius ratio of the compound jet. Chauhan et al. [21] further investigated the jet instability of compound jets using the linear temporal instability theory and found that there were two temporal growth modes, a stretching mode and a squeezing mode, and the stretching mode led to a higher growth rate than the squeezing mode. Recently, Craster et al. [22] applied the long-wave theory to study the dynamics of compound jets with a large viscosity difference between the core and shell fluids. While the linear analysis can effectively give the relationship of the growth rate and the wave number, it loses its applicability in predicting the droplet formation process when a nonlinear breakup process is involved. As an alternative approach, various numerical methods have been proposed to capture the nonlinear breakup process of compound jets. Tchavdarov et al. [23] studied the compound jets using a Lagrangian mesh-based finite element method, however this method was not able to simulate the highly deformed jet shapes. Suryo et al. [24] numerically analyzed the breakup of compound jets using the finite element method within a multiregion mesh, which conformed to and evolved with the changing breakup shape of the drop. However, this finite element method is not able to simulate the droplet formation when the jet is pinched off. Zhou et al. [25] further studied the compound droplet/microcapsule formation mechanism in microfluidic flow-focusing devices using the finite element method with adaptive meshing in a diffuse-interface framework and found that encapsulation of the inner drop depends critically on coordination of capillary waves on the inner and outer interfaces. However, the influence of only two parameters (viscosity ratio and capillary number of the inner fluid) has been studied regarding the formability of microcapsules.

While numerous studies have been conducted to investigate the double-layered microcapsule formation process using compound nozzle jetting, there is still no study to investigate how to determine the forming range of good microcapsules, which are defined as droplets with a defined core-shell structure even if the shell thickness may be nonuniform. Understanding the double-layered microcapsule formability is hindered by the limitations of the linear theory in predicting the jet breakup and of the numerical simulation in determining the perturbation growth rate as a function of wave number. To this end, this paper proposes a methodology for determining the formability of double-layered microcapsule by combining a theoretical analysis and numerical simulations. The linear instability theory-based analysis first has been implemented to obtain the relationship/curve between the growth rate ratio and the wave number. Then, a wave number range for the successful generation of double-layered microcapsules can be identified based on the growth rate ratio curve using a numerical approach. Once the good forming zone is identified, good excitation conditions, which determine the wave number, can be selectively picked without using a trial-and-error method.

3 Formability Study of Double-Layered Microcapsule in Compound Jetting

3.1 Problem Description and Process Governing Equations. Figure 1 shows a typical double-layered microcapsule fabrication system with an inner chamber/nozzle filled with a core material and an outer chamber/nozzle filled with a shell material. Sometimes a carrier stream is also introduced to facilitate double-layered microcapsule formation and droplet size control. The jet breakup process depends on the fluid properties, such as density, viscosity, and interfacial tension, as well as the excitation conditions including excitation pressure magnitudes, excitation frequencies, and carrier stream velocity. The two fluids are ejected through the nozzle

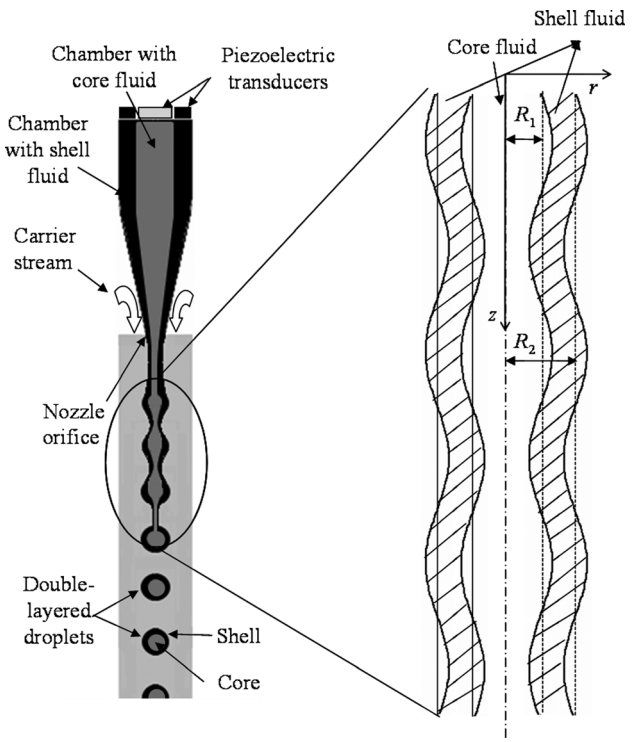

Fig. 1 Schematic of the compound nozzle and a compound jet

to form smooth and cylindrical compound jets under an external acoustic excitation generated by piezoelectric transducers. Typically, the acoustic excitation is sinusoidal and defined as follows:

$$p_{ai} = p_{ai0} - p_{ai0}\sin(2\pi f_i t) \tag{1}$$

where p_{ai} is the applied pressure, p_{ai0} is the pressure amplitude, f_i is the excitation frequency, t is the time, and i denotes a fluid ($i = 1$ represents the core fluid and $i = 2$ represents the shell fluid). The resulting wavelength λ_i is a function of excitation frequency f_i and jet velocity V_i:

$$\lambda_i = V_i/f_i \tag{2}$$

To break the compound jets into uniform droplets with a desired microsphere/droplet size, the excitation should be tuned in terms of the pressure excitation amplitude and frequency. Since the one core-one shell double-layered structure is of interest herein, the same excitation frequency was used for the core and shell fluids.

Some assumptions are introduced here to simplify the modeling process: (1) the fluids are Newtonian and incompressible, (2) the diffusion between the ambient environment and the fluid solution is negligible, (3) the shell and core polymer solutions are immiscible, (4) since the linear temporal instability analysis is of interest in this study, the Weber number is restricted to the order of 10, and (5) only the capillary-driven instability is considered, and the velocity difference across the interface of the inner and outer fluids is not sufficiently large to induce the Kelvin–Helmholtz instability. The process dynamics of the compound jet is governed by the continuity and Navier–Stokes equations as follows:

$$\frac{\partial \rho_i}{\partial t} + \nabla \cdot (\rho_i v_i) = 0 \tag{3}$$

$$\rho_i\left(\frac{\partial v_i}{\partial t} + (v_i \cdot \nabla)v_i)\right) = -\nabla p_i + \mu_i \nabla^2 v_i + F_i \tag{4}$$

where ρ_i is the fluid density of fluid i, v_i is the fluid velocity, p_i is the fluid pressure, μ_i is the fluid viscosity, and F_i is the volume force. Here and in the following, $i = 1$ (core fluid), 2 (shell fluid), and 3 (carrier stream). It should be noted that only liquid double-layered droplets formed by two immiscible core-shell fluids are of modeling interest. In practical applications, the effect of solvent evaporation/extraction or phase separation on the formability should be considered too.

3.2 Growth Rate Modeling Using Linear Temporal Instability Theory. For a typical compound jet shown in Fig. 1, a core fluid of density ρ_1 and viscosity μ_1 is surrounded by a coaxial shell fluid of density ρ_2 and viscosity μ_2. By ignoring the carrier stream effect and considering an axisymmetric, Newtonian, incompressible, and immiscible flow system, compound jetting here is studied in a polar coordinate system (r, z). Here the z-axis coincides with the core fluid axis while the r-axis is the radial axis. For high velocities applications ($V_1^2\rho_1 R_1/\sigma_1 > 3.15$), the primary and secondary modes of the spatial instability are identical to the stretching and squeezing modes [26], and only the temporal instability is examined as $V_1^2\rho_1 R_1/\sigma_1$ (of the order of 10) is larger than 3.15 in this study.

For the basic state, there is no flow, and the interfaces are cylindrical and concentric with an inner radius R_1 and an outer radius R_2. The interfacial tension of the inner interface between the core and shell fluids is σ_1, and the surface tension of the outer interface is σ_2. Here the pressure distributions are given by

$$p_1^{[0]} = 1 + \gamma/a, \quad \text{and} \quad p_2^{[0]} = \gamma/a \tag{5}$$

where the superscript [0] denotes the basic state, p_i is the nondimensional pressure scaled by σ_1/R_1 in region i, $i = 1$, and 2 in this section, $a = R_2/R_1$ is the radius ratio, and $\gamma = \sigma_2/\sigma_1$ is the interfacial tension ratio.

When the basic state is perturbed by an axisymmetric disturbance with a scale $\delta(<< 1)$, the interfacial deflections and pressure can be expanded in powers of δ,

$$f_1(z,t) = 1 + \varsigma_1^{[1]}(z,t)\delta + O(\delta^2) \tag{6}$$

$$f_2(z,t) = a + \varsigma_2^{[1]}(z,t)\delta + O(\delta^2) \tag{7}$$

$$\psi_i(r,z,t) = \psi_i^{[1]}(r,z,t)\delta + O(\delta^2) \tag{8}$$

$$p_i(r,z,t) = p_i^{[0]} + p_i^{[1]}(r,z,t)\delta + O(\delta^2) \tag{9}$$

where f_i is the location of the interfaces, ψ_i is the stream function, and the variables with a superscript [1] denote the first order terms in the expansion of δ. The nondimensional components of velocity, scaled by $(\sigma_1/(\rho_1 R_1))^{1/2}$, can be expressed in terms of stream function $\psi_i(r,z)$, scaled by $R_1^2(\sigma_1/(\rho_1 R_1))^{1/2}$, as follows:

$$u_i = \frac{1}{r}\frac{\partial \psi_i}{\partial z} \quad \text{and} \quad w_i = \frac{1}{r}\frac{\partial \psi_i}{\partial r} \tag{10}$$

where u_i and w_i are the radial and axial velocity components, respectively.

By substituting the expansion of the stream function (Eq. (8)) into the Navier–Stokes equation and retaining the first order terms in δ, a linear differential equation for $\psi_i^{[1]}(r,z,t)$ can be obtained. Further using the Fourier transform along the z direction introduces a wave number k, and using the Laplace transform in time introduces a growth rate variable s, which characterizes how fast the jet instability grows upon disturbance and is a function of wave number, then the jetting system is represented by [21]

$$D\left(D - \frac{J^{1/2}b_i s}{m_i}\right)\psi_i(r,k,s) = 0 \tag{11}$$

with the operator D defined by

$$D = \frac{d^2}{dr^2} - \frac{1}{r}\frac{d}{dr} - k^2$$

and some dimensionless parameters $J = \rho_1\sigma_1 R_1/\mu_1^2$, which is $1/\mathrm{Oh}^2$, where the Ohnesorge number Oh is defined as $\mu/\sqrt{\rho_1\sigma_1 R_1}$, $m_1 = \mu_1/\mu_1 = 1$, $m = m_2 = \mu_2/\mu_1$ is the viscosity ratio, $b_1 = \rho_1/\rho_1 = 1$, and $b = b_2 = \rho_2/\rho_1$ is the density ratio. The associated boundary conditions are given as follows [21]:

(1) At $r/R_1 = 0$, the velocity is bounded,

$$\psi_1 < \infty, \quad \text{and} \quad \frac{d\psi_1}{dr} < \infty \tag{12}$$

(2) At $r/R_1 = 1$, the velocity is continuous, the tangential stresses are equal, the normal stresses balance the capillary force, and there is no phase separation at the inner interface,

$$\psi_1 = \psi_2 \tag{13}$$

$$\frac{d\psi_1}{dr} = \frac{d\psi_2}{dr} \tag{14}$$

$$m(D\psi_2 + 2k^2\psi_2) = D\psi_1 + 2k^2\psi_1 \tag{15}$$

$$\frac{m}{ikr}\frac{d}{dr}\left[\left(D - sJ^{1/2}\frac{b}{m}\right)\psi_2\right] + 2mik\frac{d}{dr}\left[\frac{1}{r}\psi_2\right] - \frac{1}{ikr}\frac{d}{dr}\left[\left(D - sJ^{1/2}\right)\psi_1\right] - 2ik\frac{d}{dr}\left[\frac{1}{r}\psi_1\right] = J^{1/2}\left[k^2 - 1\right]\zeta_1 \tag{16}$$

where

$$\zeta_1 = \frac{ik\psi_1}{s} + \frac{\zeta_{1,0}}{s}$$

and $\zeta_{1,0}$ is the Fourier transform of the initial deflection $\zeta_{1,0}^{[1]}(z)$.

(3) At $r/R_1 = a$, the tangential stress is zero, the normal stresses balance the capillary force, and there is no phase separation at the outer interface,

$$D\psi_2 + 2k^2\psi_2 = 0 \tag{17}$$

$$\frac{m}{ikr}\frac{d}{dr}\left[\left(D - sJ^{1/2}\frac{b}{m}\right)\psi_2\right] + 2mik\frac{d}{dr}\left[\frac{1}{r}\psi_2\right] = -\gamma J^{1/2}\left[k^2 - \frac{1}{a^2}\right]\zeta_2 \tag{18}$$

where

$$\zeta_2 = \frac{ik\psi_2}{as} + \frac{\zeta_{2,0}}{s}$$

and where $\zeta_{2,0}$ is the Fourier transform of the initial deflection $\zeta_{2,0}^{[1]}(z)$.

From Eq. (11), ψ_i is found as $A_i rI_1(kr) + B_i rK_1(kr) + D_i rI_1(\beta_i r) + E_i rK_1(\beta_i r)$, where I_1 and K_1 are the modified Bessel function of order one, $\beta_i^2 = k^2 + sJ^{1/2}b_i/m_i$, and A_i, B_i, D_i, and E_i are the integration constants. By substituting the solution ψ_i into the above boundary conditions, the system dynamics can be described as $A(k,s)_{8\times 8}x(k,s) = b(k)$, where the coefficient matrix $(A(k,s))$ is an 8×8 matrix, $x(k,s)$ is the column vector $[A_2 \quad B_2 \quad D_2 \quad E_2 \quad A_1 \quad D_1 \quad -j\zeta_1 \quad -j\zeta_2]^T$, $b(k)$ is the column vector $[0 \quad 0 \quad 0 \quad 0 \quad 0 \quad 0 \quad j\zeta_{1,0} \quad j\zeta_{2,0}]^T$, and j is the standard imaginary unit. The growth rates $(s(k))$ are the roots of the dispersion equation, $\det(A(k,s)) = 0$. Among the roots of the dispersion equation, two solutions, which tend to be zero as k approaches zero, are unstable. The two modes correspond to two different jet configurations, stretching and squeezing, as shown in Fig. 2. In the stretching mode, the two interfaces grow in phase, which is desirable for compound drop formation; in the squeezing mode, the two interfaces grow out of phase, which leads to unmatched breakup of the inner and outer jets, forming disorderly droplets.

3.3 Formability Prediction Using Linear Temporal Instability Theory and Numerical Simulation. As aforementioned, two growth modes may coexist for a compound jet, the stretching mode for in-phase growth and the squeezing mode for out-of-phase growth. The growth rate ratio, defined as the ratio of the squeezing growth rate to the stretching growth rate, is introduced here to characterize the competition between the two modes during the formation process of microcapsules. Within the stretching and squeezing co-occurrence region, the growth rate ratio measures the dominance of the squeezing mode over the stretching mode. Based on the growth rates estimated from the dispersion equation, a typical growth rate ratio curve is obtained and shown in Fig. 3, where $k_{l\max}$ is the local maximum, illustrating the dominance of the squeezing mode. Within the region as $k \to 0$, the stretching growth rate is too small to form good microcapsules within a given duration. Within the region close to $k_{l\max}$, the growth rate of the stretching mode is not large enough to overshadow that of the squeezing mode since the growth rate of the squeezing mode becomes pronounced too. Thus, the inner and outer interfaces grow out of phase, resulting in irregular droplets. Within the low wave number $(0, k_{l\max}]$ region, microcapsules cannot be efficiently formed within a fixed spatial domain or a given jetting/printing distance. As such, the wave number range of $[k_{l\max},1]$ is strategically picked to determine the lower (k_l) and upper (k_u) bounds, which collectively define the good formability range of double-layered microcapsules, and k_l and k_u can be determined as follows.

The lower bound (k_l) is determined from the co-occurrence region $((k_{l\max}, k_0])$ where both the stretching and squeezing modes exist. Here k_0 is picked as $1/a$, where the squeezing mode disappears. Generally, the lower bound of the formability region, k_l, is larger than $k_{l\max}$, and this critical wave number, k_l, can be determined using a pseudobisection method in conjunction with a numerical simulation method as follows: (1) First, a growth rate ratio curve such as Fig. 3 is obtained based on the dispersion equation using the linear instability theory. (2) Second, the droplet formation process is numerically simulated at the wave number k_1, which is a median value between $k_{l\max}$ and k_0 as $(k_0 + k_{l\max})/2$, and the formability at k_1 is examined. The wave number can be tuned by changing the jet velocity V_1 and the excitation frequency f based on the relationship $k = (2\pi f/V_1)R_1$ using the $V_1 = f\lambda_1$ estimation per the simulation results. The jet velocity V_1 is not sensitive to frequencies once the excitation pressure and the material properties are given. In this numerical simulation, the wave number was tuned by changing the excitation frequency only. (3) If good microcapsules as visually observed are formed at k_1, the previous step is repeated at a wave number $k_2 = (k_1 + k_{l\max})/2$, otherwise, at a wave number $k_2 = (k_1 + k_0)/2$. In other words, a subsequent wave number is chosen based on a left-side median

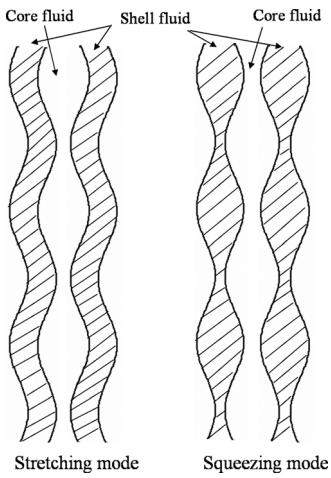

Fig. 2 Schematic of the stretching and squeezing modes with inner and outer interfaces illustrated

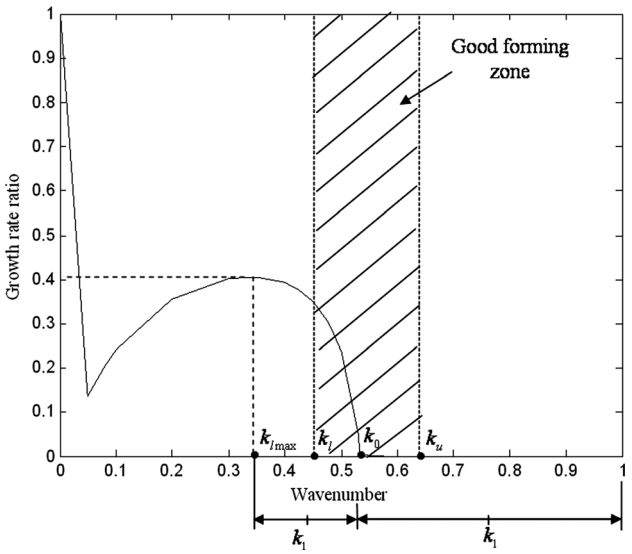

Fig. 3 The growth rate ratio with respect to the wave number

value for a good formation case at the current wave number, otherwise, a right-side median value. (4) This process is iterated until a specified resolution (the difference between the current and subsequent wave numbers) is reached, and the current wave number is called as k_l, a lower formability bound.

The upper bound (k_u) is determined from stretching-only region ($[k_0, 1)$) where only the stretching mode exists. Generally, the upper bound of the formability region, k_u, is larger than k_0 but smaller than 1, and this critical wave number (k_u) can also be determined based on a pseudobisection method in conjunction with a numerical simulation method as follows: (1) First, a growth rate ratio curve such as Fig. 3 is obtained based on the dispersion equation using the linear temporal instability theory. (2) Second, the droplet formation process is numerically simulated at the wave number k_1, which is a median value between k_0 and 1 as $k_1 = (k_0 + 1)/2$, and the formability at k_1 is examined. (3) If good microcapsules are formed at k_1, the previous step is repeated at a wave number $k_2 = (k_1 + 1)/2$; otherwise, at a wave number $k_2 = (k_0 + k_1)/2$. In other words, a subsequent wave number is chosen based on a right-side median value for a good formation case at the current wave number, otherwise, a left-side median value. (4) This process is iterated until a specified resolution (the difference between the current and subsequent wave numbers) is reached, and the current wave number is called as k_u, an upper formability bound.

Within the determined $[k_l, k_u]$ range, any wave number leads to good double-layered microcapsules/compound droplets. It should be noted that the growth rate ratio curve depends on the parameters, a, b, m, γ, and J, so the range $[k_l, k_u]$ may be different for different parameter combinations and the formability prediction process needs to be repeated for each parameter combination.

4 Implementation and Case Study of Formability Prediction

4.1 Jetting System Setup. Based on the linear temporal instability analysis, a jet will eventually break up, maybe after a long duration, even if the magnitude of growth rate is small. However, in practice, there usually is a limited spatial domain for the generation of droplets. It is always expected that good droplets form within a certain spatial distance (printing or direct-writing height) from an orifice. The compound jet formation process was studied as a two-dimensional problem due to its axisymmetric characteristics as shown in Fig. 4.

The radii of the inner and outer inlets were 25 and 50 μm, respectively, the length of the solution chamber was 600 μm, the radii of the inner (R_1) and outer (R_2) orifice were 16 and 30 μm, respectively, and the carrier stream domain had a radius of 100 μm and a length of 1500 μm. For this study, water was picked as the core fluid, 3% (w/v) poly (lactide-co-glycolide) (PLGA) in ethyl acetate (EA) [15] was picked as the shell fluid, and their materials properties are listed in Table 1. The carrier stream in this study was air with a density of 1.2 kg/m^3 and a viscosity of 0.018 mPa s. The core fluid-shell fluid interfacial tension is approximately equal to the difference of the surface tension of the core fluid-air and that of the shell fluid-air, so the core fluid-air surface tension was determined from the core fluid-shell fluid interfacial tension and the shell fluid-air surface tension values from Table 1. To simplify the simulation problem, the pressure amplitude of the core fluid (p_{a10}) was 0.11 MPa, the pressure amplitude of the shell fluid (p_{a20}) was 0.09 MPa, and the air inlet velocity was 0 m/s. The pressure excitations of the core and shell fluids were in phase.

4.2 Numerical Simulation Using VOF Method. Numerical simulations are needed in determining the lower and upper bounds. The aforementioned microcapsule formation process involved two-phase fluids, namely two liquid components (core fluid and shell fluid) and a gas phase (carrier stream). The interface between the core and shell fluids and the interface between the shell fluid and the carrier stream were modeled using a volume of fluid (VOF) method, a surface-tracking technique applied to a fixed Eulerian mesh to track the moving interfaces per its applicability in modeling droplet formation [11]. In the VOF method, multiple immiscible fluids are simulated by solving the continuity, momentum, and volume fraction equations. The tracking of the interfaces between fluid phases was implemented by solving a continuity equation for the volume fraction of each phase.

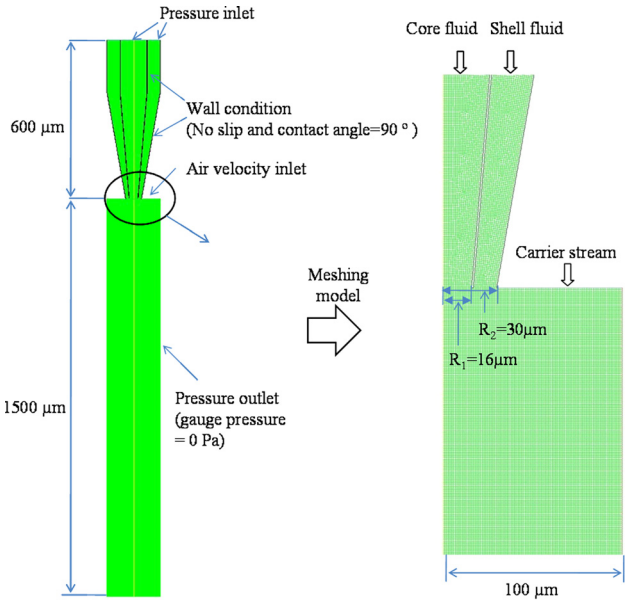

Fig. 4 Computational domains setup

Table 1 Material properties of the core and shell fluids

	Density (kg/m^3)	Viscosity (Pa · s)	Core-shell interfacial tension (N/m)	Surface tension (N/m)
Core fluid	997.1 [15]	0.000890 [15]	0.068	N.A.
Shell fluid	894.6 [15]	0.001237 [15]	0.068	0.0735

During simulations, the walls that enclosed both the liquids inside the chamber, respectively, were considered as a wall boundary condition with no slip and their contact angles were 90 deg. The excitation pressures were employed as a pressure boundary condition at the chamber inlets. To satisfy the convergence requirement, the time step was taken as 0.01 μs and the mesh size was taken on the order of 1 μm based on a sensitivity test. In the computational domain, 200,378 quadrilateral elements were used. The algorithm using a first-order upwind scheme, and noniterative time advancement was implemented also based on a sensitivity test. For computational stability, the implicit algorithm was used in this study to solve the governing equations. It should be pointed out that the VOF method was implemented using the explicit algorithm to make the geometric reconstruction scheme available. The simulation was performed using FLUENT 6.3.

Figure 5 shows the typical simulation results under two excitation frequencies, 50 and 60 kHz. The material properties and excitation conditions for the two cases are shown in Table 2. For case 1, the material properties from Table 1 were directly used, while for case 2 some material properties and operating conditions were changed to show the effects of material properties and operating conditions on droplet formation. The simulation results of droplet formation were taken at the time $t = 400$ μs and both cases were successful in generating good microcapsules. It can be seen that

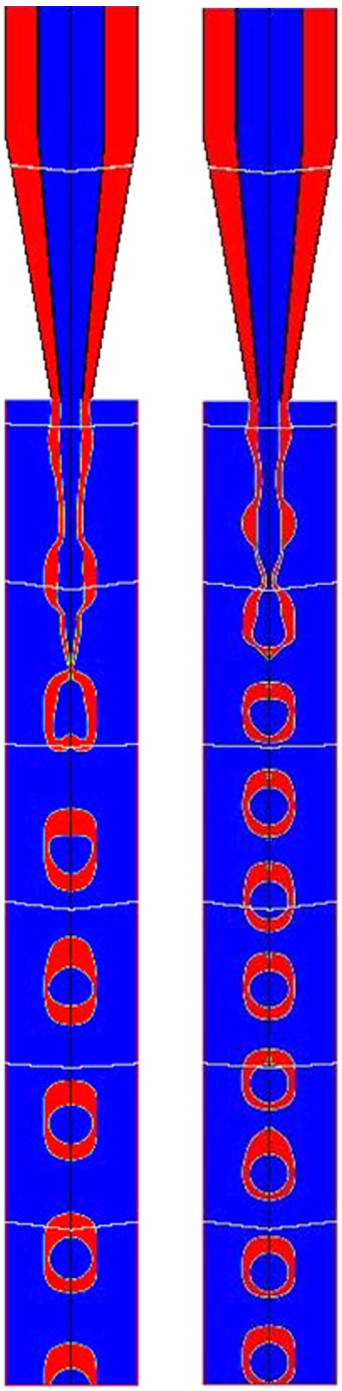

Fig. 5 Representative simulation results of compound jetting (*a*) case 1 (50 kHz) and (*b*) case 2 (60 kHz) (the microcapsule structure might be best viewed in a colored display)

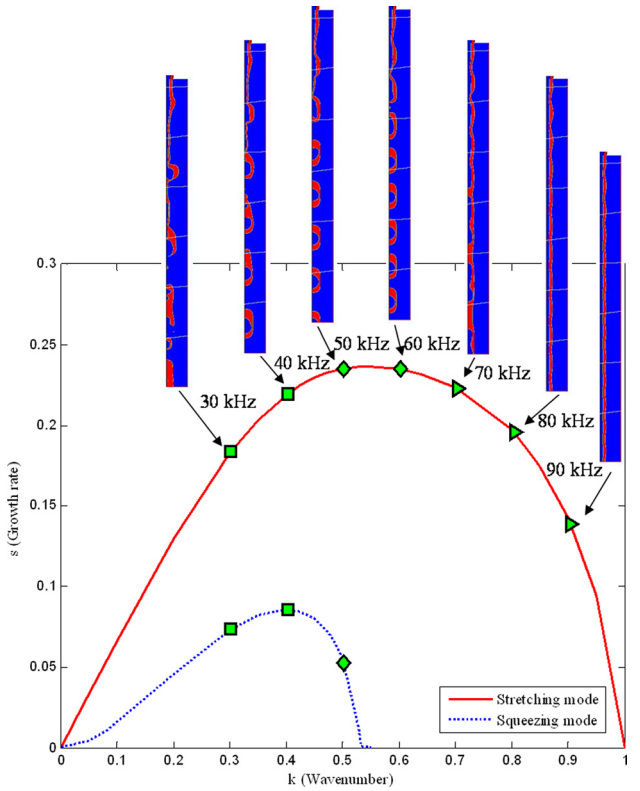

Fig. 6 Growth rate as a function of wave number and some representative simulation results (radius ratio $a = 1.87$, density ratio $b = 0.87$, interfacial tension ratio $\gamma = 1.08$, and viscosity ratio $m = 1.38$ as specified in Table 1)

(1) more droplets were obtained in the case of frequency 60 kHz (case 2) than that of frequency 50 kHz (case 1) and (2) the droplets of case 1 were larger than those of case 2. These observations are attributed to (1) a higher frequency leads to a shortened droplet formation period. For the same time duration, more droplets break up from the liquid jet under a high frequency excitation, and (2) a larger viscosity decreases the jet velocity. As a result, the liquid volume within one wavelength is smaller, leading to smaller droplets. The dependency of the droplet size on the excitation frequency and the liquid viscosity is similar to that observed during single nozzle jetting [11].

4.3 Prediction of Double-Layered Microcapsule Formability. Figure 6 shows the growth rates as a function of wave number derived based on the dispersion equation and some numerical simulation results based on the material properties given in Table 1. Some simulation results are listed for illustration by varying the excitation frequency from 30 to 90 kHz with an interval of 10 kHz. Under the given frequency range there are two unstable modes, stretching and squeezing. The stretching mode is unstable for all wavelengths greater than the undisturbed core circumference ($k \in (0, 1)$) and tends to make the two interfaces grow or stretch in phase. This stretching growth finally causes breakup of the core and shell fluids to form microcapsules.

Table 2 Material properties and excitation conditions for the two cases

Case	Core pressure (Pa)	Shell pressure (Pa)	Excitation frequency (Hz)	Core viscosity (Pa · s)	Interfacial tension (N/m)	Shell viscosity (Pa · s)	Shell surface tension (N/m)
1	9×10^4	1.1×10^5	5×10^4	0.00089	0.068	0.001237	0.07350
2	9×10^4	1.2×10^5	6×10^4	0.00178	0.136	0.002474	0.03675

Table 3 Growth rates under different excitation frequencies

		Growth rate calculated using the dispersion equation	
Frequency (kHz)	Wave number	Stretching mode	Squeezing mode
30	0.3016	0.18357	0.07360
40	0.4021	0.21947	0.08600
50	0.5027	0.23544	0.05278
60	0.6032	0.23494	0
70	0.7037	0.22301	0
80	0.8042	0.19572	0
90	0.9048	0.13880	0

Generally, the stretching mode tends to achieve an ideal microcapsule. In contrast, the growth rate in the squeezing mode is positive when $k < 1/a$ or zero when $k > 1/a$, implying that the jet is unstable if the wavelength is greater than the undisturbed shell circumference ($k \in (0, 1/a)$). The squeezing mode tends to make the two interfaces grow out of phase, leading to disordered droplet breakup. Table 3 lists the wave numbers determined using FLUENT and the resulting growth rates determined using the dispersion equation. The wavelength was measured from the phase simulation contour and calculated from the stable jet velocity and the excitation frequency, both giving comparable wavelengths for good compound jets, so all the wavelengths were calculated from the stable jet velocity and the excitation frequency. Then the wave number was determined by dividing $2\pi R_1$ by the calculated wavelength.

Figure 7, which uses the growth rate ratio as the formability indicator, is the alternative representation of Fig. 6. A predicted forming zone of good microcapsules is marked as Region II. The presented simulation results represent the iteration process to find the lower and upper bounds using the proposed pseudobisection method. In practical implementation, only Fig. 7 needs to be constructed using the proposed formability prediction approach, and the predicted forming range can be further validated using the results similarly as shown in Fig. 6. Three regions shown in Fig. 7, including one good forming (Region II) and two unsatisfactory forming (Regions I and III) regions, can be determined by

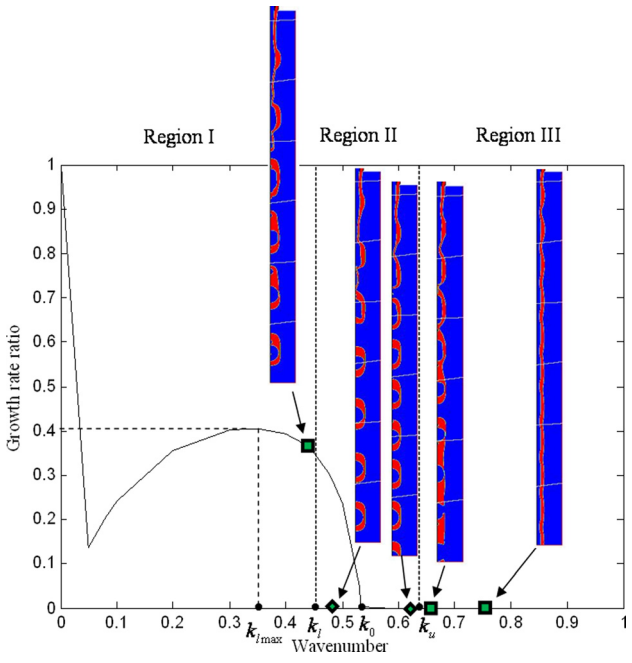

Fig. 7 Growth rate ratio as a function of wave number and some simulation results using the same material properties and nozzle geometry as for Fig. 6

the proposed approach using both the linear temporal instability theory and numerical simulations. Region I corresponds to low wave numbers, where both the stretching and squeezing modes come into play, resulting in irregular microcapsules. Region II corresponds to wave numbers within the forming wave number range, [0.37, 0.65], where the stretching mode is dominant and the growth rate is near the peak value. The droplets are uniformly broken up away from the jet. Region III corresponds to the high wave number region, where only the stretching mode exists. However, the stretching growth rate is small, and it takes a long time for the jet to break up into droplets. The droplet breakup is not observed due to the weak perturbation as shown in Fig. 7.

4.4 Discussion. The linear instability analysis can be used to understand the coexistence of two temporal growth modes (stretching and squeezing) during compound jetting. The stretching mode is unstable for wavelengths greater than the undisturbed inner circumference ($0<k<1$), in which the two interfaces grow in phase. The squeezing mode is unstable for wavelengths greater than the outer circumference ($0<k<a$), in which the two interfaces grows exactly out of phase. The growth rates of the stretching and squeezing modes together determine the formability of microcapsules. Generally, a large growth rate of the stretching mode facilitates the generation of regular or good microcapsules since the inner and outer interfaces grow in phase. In contrast, a large growth rate of the squeezing mode may lead to the generation of irregular microcapsules since the two interfaces grow out of phase. Within a good forming zone defined by wave numbers, the outer interface grows in phase with the inner interface and ultimately breaks up and generates good compound droplets although the wavelength may be smaller than the outer circumference. Under the effect of the stretching mode, the interface growth, when it is beyond the linear region, results in the breakup of the core fluid, so the primary droplets formed by the core fluid are surrounded by the shell fluid. When the instability continues to grow, the further nonlinear stretching causes the shell fluid to break up, forming compound droplets or double-layered microcapsules. Hertz and Hermanrud [27] have experimentally studied a compound jet breakup process, and it can be interpreted from their experimental observations that good compound droplets formed at the average wave number around 0.6. While different fluids were studied, this wave number falls into the identified good forming zone of the aforementioned case study ([0.37, 0.65]). More experimental studies are expected to validate and improve the proposed prediction methodology in future studies upon the development of advanced compound jetting apparatuses.

5 Conclusions

This study has proposed a novel methodology to predict the formability of double-layered microcapsules/compound droplets in compound nozzle jetting by combining a theoretical analysis with numerical simulations. A linear temporal instability analysis is used to define the perturbation growth rates of stretching and squeezing modes and a growth ratio as a function of the wave number, and a computational fluid dynamics (CFD) method is implemented to model the microcapsule formation process in order to determine the good microcapsule forming range based on the growth ratio curve. The lower and upper bounds of the good formability range have been determined using a pseudobisection method based on both the stretching and squeezing modes for a given materials-nozzle system. The proposed formability prediction methodology has been implemented in modeling a water-poly (lactide-co-glycolide) (PLGA)-air compound jetting system.

The resulting knowledge helps to understand the formability of double-layered microcapsule fabrication in compound jetting. While the one core-one shell double-layered structure is studied here, it should be pointed out that the resulting knowledge also applies to multicore-one shell double-layered structures. Since the VOF method is still questioned about its capacity in predicting

droplet formation, it is suggested that new numerical methods should be incorporated in the future in addition to VOF. It is recognized that the proposed methodology cannot be readily implemented; as such, future work should also focus on producing dimensionless phase diagrams for microcapsule formability.

Acknowledgment

The work was partial supported by the National Science Foundation (CMMI-1100402 and EPS-0903795) and the National Institutes of Health (P20RR016461). The authors would like to thank Dr. Scott Little and Dr. Joann Sullivan for their continued support.

References

[1] Lee, S. J., and Rosenberg, M., 2000, "Whey Protein-Based Microcapsules Prepared by Double Emulsification and Heat Gelation," Lebensm.-Wiss. u.-Technol., **33**, pp. 80–88.
[2] Langer, R., 1998, "Drug Delivery and Targeting," Nature, **392**(Suppl. 6679), pp. 5–10.
[3] Loscertales, I. G., Barrero, A., Guerrero, I., Cortijo, R., Marquez, M., and Gañán-Calvo, A. M., 2002, "Micro/Nano Encapsulation via Electrified Coaxial Liquid Jets," Science, **295**, pp. 1695–1698.
[4] López-Herrera, J. M., Barrero, A., López, A., Loscertales, I. G., Márquez, M., 2003, "Coaxial Jets Generated From Electrified Taylor Cones. Scaling Laws," Aerosol Sci., **34**, pp. 535–552.
[5] Utada, A. S., Lorenceau, E., Link, D. R., Kaplan, P. D., Stone, H. A., and Weitz, D. A., 2005, "Monodisperse Double Emulsions Generated From a Microcapillary Device," Science, **308**, pp. 537–541.
[6] Bocanegra, R., Sampedro, J. L., Gañán-Calvo, A., and Marquez, M., 2005, "Monodisperse Structured Multi-Vesicle Microencapsulation Using Flow-Focusing and Controlled Disturbance," J. Microencapsulation, **22**(7), pp. 745–759.
[7] Berkland, C., Pollauf, E., Varde, N., Pack, D. W., and Kim, K., 2007, "Monodisperse Liquid-Filled Biodegradable Microcapsules," Pharm. Res., **24**(5), pp. 1007–1013.
[8] Yeo, Y., Chen, A. U., Basaran, O. A., and Park, K., 2004, "Solvent Exchange Method: A Novel Microencapsulation Technique Using Dual Microdispensers," Pharm. Res., **21**, pp. 1419–1427.
[9] Jain, R. A., 2000, "The Manufacturing Techniques of Various Drug Loaded Biodegradable Poly(lactide-co-glycolide) (PLGA) Devices," Biomaterials, **21**, pp. 2475–2490.
[10] Berkland, C., Pollauf, E., Pack, D. W., and Kim, K., 2004, "Uniform Double-Walled Polymer Microspheres of Controllable Shell Thickness," J. Controlled Release, **96**(1), pp. 101–111.
[11] Herran, C. L., Wang, W., Huang, Y., Mironov, V., and Markwald, R., 2010, "Parametric Study of Acoustic Excitation-Based Glycerol-Water Microsphere Fabrication in Single Nozzle Jetting," ASME J. Manuf. Sci. Eng., **132**(5), p. 051001.
[12] Scheele, G. F., and Meister, B. J., 1968, "Drop Formation at Low Velocities in Liquid-Liquid Systems: Part 1. Prediction of Drop Volume," AIChE J., **14**, pp. 9–15.
[13] Utada, A. S., Fernandez-Nieves, A., Stone, H. A., and Weitz, D. A., 2007, "Dripping to Jetting Transitions in Coflowing Liquid Streams," Phys. Rev. Lett., **99**, p. 094502.
[14] Chu, L. Y., Utada, A. S., Shah, R. K., Kim, J. W., and Weitz, D. A., 2007, "Controllable Monodisperse Multiple Emulsions," Angew. Chem. Int. Ed., **46**, pp. 8970–8974.
[15] Lee, S. Y., Snider, C., Park, K., and Robinson, J. P., 2007, "Compound Jet Instability in a Microchannel for Mononuclear Compound Drop Formation," J. Micromech. Microeng., **17**, pp. 1558–1566.
[16] Snider, C., Lee, S. Y., Yeo, Y., Grégori, G. J., Robinson, J. P., and Park, K., 2008, "Microenvironment-Controlled Encapsulation (MiCE) Process: Effects of PLGA Concentration, Flow Rate, and Collection Method on Microcapsule Size and Morphology," Pharm Res., **25**(1), pp. 5–15.
[17] Chang, F. C., and Su, Y. C., 2008, "Controlled Double Emulsification Utilizing 3D PDMS Microchannels," J. Micromech. Microeng., **18**, p. 065018.
[18] Tomotika, S., 1935, "On the Instability of a Cylindrical Thread of a Viscous Liquid Surrounded by Another Viscous Fluid," Proc. R. Soc. London, Ser. A, Math. Phys. Sci., **150**, pp. 322–337.
[19] Sanz, A., and Meseguer, J., 1985, "One-Dimensional Linear Analysis of the Compound Jet," J. Fluid Mech., **159**, pp. 55–68.
[20] Shkadov, V. Y., and Sisoev, G. M., 1996, "Instability of a Two-Layer Capillary Jet," Int. J. Multiphase Flow, **22**(2), pp. 363–377.
[21] Chauhan, A., Maldarelli, C., Papageorgiou, D. T., and Rumschitzki, D. S., 2000, "Temporal Instability of Compound Threads and Jets," J. Fluid Mech., **420**, pp. 1–25.
[22] Craster, R. V., Matar, O. K., and Papageorgiou, D. T., 2005, "On Compound Liquid Threads With Large Viscosity Contrasts," J. Fluid Mech., **533**, pp. 95–124.
[23] Tchavdarov, B., Minev, P. D., and Radev, S., 1994, "Numerical Analysis of Compound Jet Disintegration," Comput. Methods Appl. Mech. Eng., **118**, pp. 121–132.
[24] Suryo, R., Doshi, P., and Basaran, O. A., 2006, "Nonlinear Dynamics and Breakup of Compound Jets," Phys. Fluids, **18**, p. 082107.
[25] Zhou, C., Yue, P., and Feng, J. J., 2006, "Formation of Simple and Compound Drops in Microfluidic Devices," Phys. Fluids, **18**, p. 092105.
[26] Chauhan, A., Maldarelli, C., Papageorgiou, D. T., and Rumschitzki, D. S., 2006, "The Absolute Instability of an Inviscid Compound Jet," J. Fluid Mech., **549**, pp. 81–98.
[27] Hertz, C. H., and Hermanrud, B., 1983, "A Liquid Compound Jet," J. Fluid Mech., **131**, pp. 271–287.